Supplement of Atmos. Chem. Phys., 20, 15297–15306, 2020
https://doi.org/10.5194/acp-20-15297-2020-supplement

Atmospheric Chemistry and Physics
Open Access

Supplement of

Sensitivity of warm clouds to large particles in measured marine aerosol size distributions – a theoretical study

Tom Dror et al.

Correspondence to: Ilan Koren (ilan.koren@weizmann.ac.il) and J. Michel Flores (flores@weizmann.ac.il)

Contents of this file

1. Text S1 to S8
2. Figures S1 to S8

Introduction

Here we show all of the marine aerosol size distributions (MSDs) that were used as inputs to the model (Text S1; Fig. S1), and the outputs of the model (i.e., rain yield and cloud's maximum mass) for the two shallower profiles used (Text S2; Fig. S2). In addition, to gain a better understanding of the non-monotonic behavior of the surface rain yield and cloud's maximum mass as a function of aerosol concentration (N_{tot}), we examined the time evolution of condensation–evaporation, collision–coalescence, and surface rain for the *Pacific–6* MSD (which does not contain giant or ultragiant particles; Text S3, Fig. S3). We also show, that the *Atlantic–1* MSD has no optimal aerosol concentration (N_{op}) by running the model with N_{tot} of up to $10^6\,cm^{-3}$ (Text S4; Fig. S4). We examine the time evolution of the total droplet surface area for all MSDs at four different N_{tot} (Text S5; Fig. S5), and we investigate the droplet size distributions below cloud base for all MSDs for $N_{tot} = 2629\,cm^{-3}$ (Text S6; Fig. S6). Finally, we examine the time-height evolution of the horizontal mean profiles of key parameter of the clouds (Text S7–S8; Figs. S7–S8).

Text S1. Normalized MSDs. Six measured MSDs that represent a variety of different marine environments were normalized to the other five MSD concentrations (total of 36 MSDs). This allowed for a careful examination of the effect of both N_{tot} and the MSD's shape. Figure S1 shows all MSDs. The *Atlantic–1* and the *Atlantic–2* are the only MSDs that contained GCCN, and the *Atlantic–1* is the only MSD that contained UGCCN. Note that even though the *Atlantic—2* contained some GCCN, they were present at low concentrations ($1.6 \times 10^{-6} - 7.5 \times 10^{-5}\, cm^{-3}$, for the lowest and highest N_{tot}, respectively). These concentrations of GCCN are low in comparison to e.g., the GCCN concentration of the *Atlantic–1* MSD ($1.9 \times 10^{-5} - 5.7 \times 10^{-4}\, cm^{-3}$), and are not sufficient to cause any effect on the *Atlantic–2* rain formation and growth.

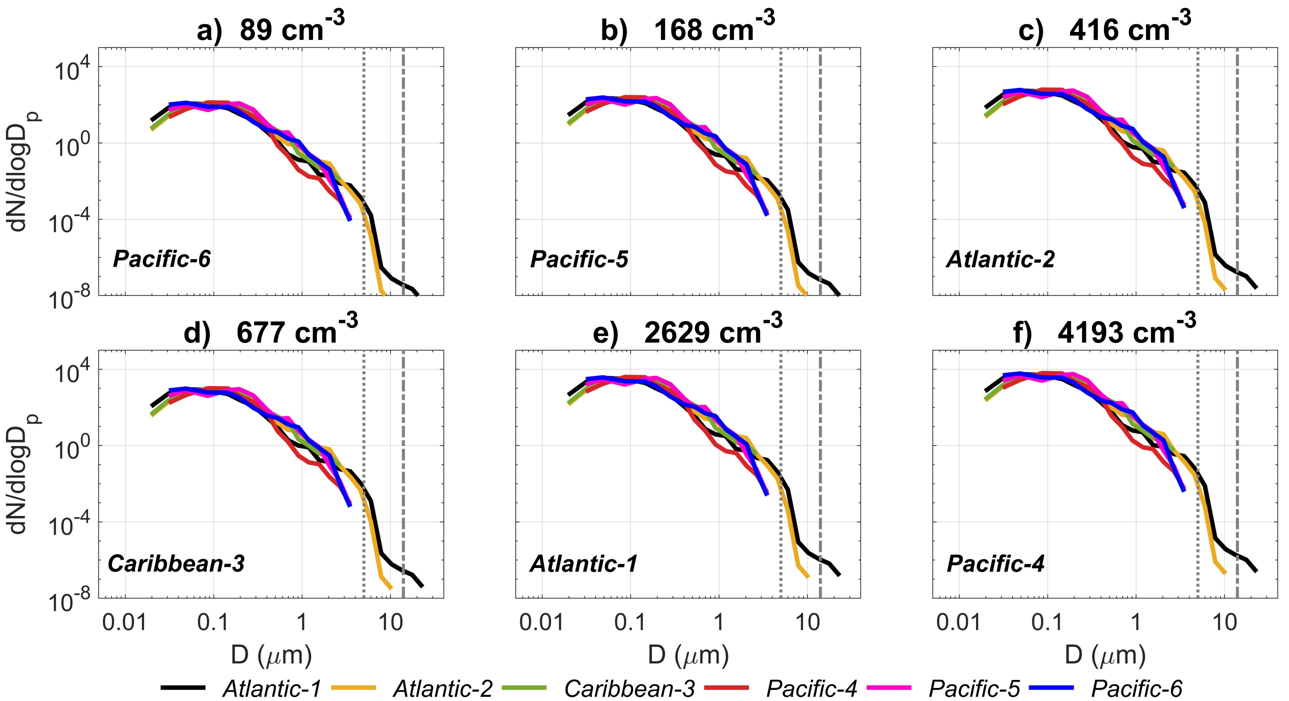

Figure S1. All of the MSDs used in the model. Each panel shows the MSDs normalized to the specific total aerosol concentration of the MSD noted in the lower left corner. The panels are organized from clean (a) to polluted (f) conditions. Dotted and dash-dotted verticals line indicate the threshold for GCCN ($D_p = 5\,\mu m$) and UGCCN ($D_p = 14\,\mu m$), respectively.

Text S2. Additional Atmospheric Profiles. To examine the effect of the different MSDs on cloud properties over a range of atmospheric conditions, we ran the model with three different sets of initial thermodynamic conditions. The initial conditions were based on idealized atmospheric profiles describing a tropical moist environment (Garstang and Betts, 1974; Dagan et al., 2015). The three profiles are presented in Figure 1 of Dagan et al. (2015) and include: a well mixed sub-cloud layer between 0 and $\sim 1000\,m$ and a conditionally unstable cloudy layer between 1000 and $4000\,m$ (deep), $3000\,m$ (intermediate), and $2000\,m$ (shallow). The profiles were bounded by an overlying inversion layer with a temperature gradient of 2^oC over $50\,m$. Three different dewpoint temperatures were assigned to the profiles such that the relative humidity (RH) in the cloudy layer was 95%, 90%, and 80%, respectively. We examined the surface rain yield and the cloud's maximum mass as a function of N_{tot}. The results of the deepest cloud profile are shown in the main text (Fig. 2a–b), and the the other two profiles are shown in Fig. S2. The trends of the *Atlantic—1* surface rain yield and cloud's maximum mass curves for the intermediate profile are similar to the ones of the deeper profile. The only difference is that the rain yield values of the *Atlantic—1* are higher than the ones produced by the other MSDs for $N_{tot} > 677\,cm^{-3}$. All the curves show a lower N_{op} compared to the deepest profile curves. Under the shallow thermodynamic profile, the *Atlantic—1* rain yield curve shows a similar trend to all other MSD cases, while producing the highest rain values. As for the trend in cloud mass, the *Atlantic—1* shows a monotonic increase (similar to the deep and intermediate profiles). The behavior of surface rain yield and the cloud's maximum mass as a function of N_{tot} strongly depends on the environmental conditions, i.e., the more unstable the profile (e.g., higher inversion height and RH in the cloudy layer), the more salient the revealed effect of the MSD. In all cases, the *Atlantic–1* clouds have a distinctively different behavior compared to the rest of the MSDs.

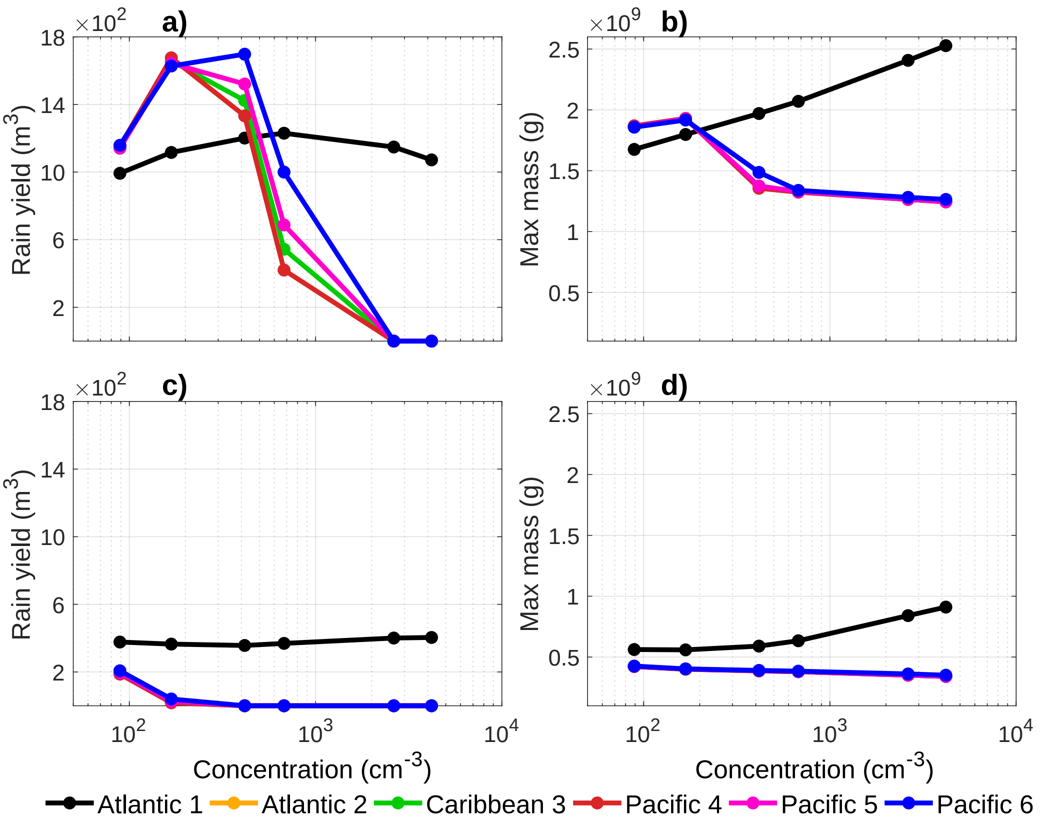

Figure S2. Surface rain yield (a and c) and cloud's maximum mass (b and d) as a function of N_{tot} for the intermediate and shallow profiles. The top panels refer to an inversion height of $3000\,m$ and a RH of 90% in the cloudy layer. The lower panels refer to an inversion height of 2000 m with 80% RH in the cloudy layer. Each curve represents six simulations with a specific shape of the MSD normalized to a different N_{tot}.

Text S3. Cloud's Microphysical Processes. To understand the non-monotonic behavior of the surface rain yield and cloud's maximum mass as a function of N_{tot}, we examined the time evolution of condensation–evaporation, collision-coalescence, and surface rain as the three major cloud processes. Figure S3 shows these processes for three different N_{tot} (clean, optimum and polluted conditions) using the *Pacific–6* MSD. The timing and the interaction between the processes are evident between the different clouds shown in Fig. SS3. As N_{tot} increases (and the total droplet surface area becomes larger), so does the condensation efficiency (Pinsky et al., 2013; Seiki and Nakajima, 2014), and the collision–coalescence process is delayed. For the clean cloud, the early onset of collision–coalescence acts to further reduce the droplets' surface area, and triggers the early formation of rain. The more polluted the cloud is, the longer the time it has to grow by condensation (i.e., the peak in collision-coalescence drifts further away from the peak of condensation–evaporation). On the other hand, the delay in collision–coalescence allows entrainment processes to act for a longer time, resulting in enhanced evaporation. The cloud presented in Fig. S3b shows the evolution and interaction of these processes under an optimal N_{tot} (N_{op}), for which the cloud mass (not shown) and surface rain yield are maximal. For the N_{op} scenario, the timing of the different cloud processes is ideal for cloud growth and rain-out (Dagan et al., 2015).

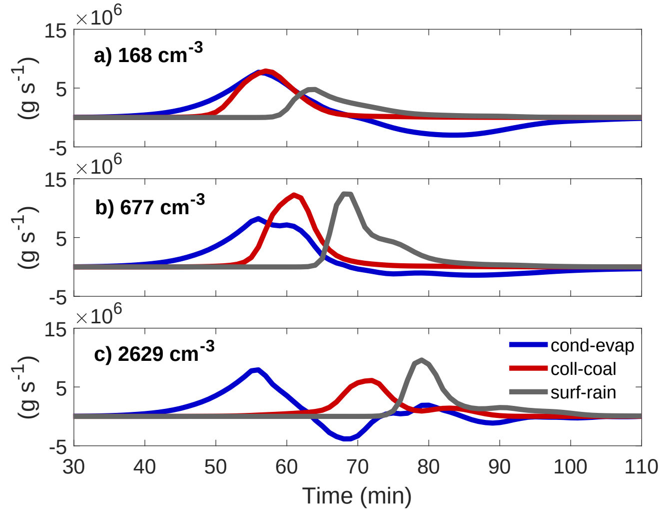

Figure S3. Total condensed–evaporated mass (blue), collected mass (red), and surface rain mass (gray) per unit time, as a function of time for the *Pacific–6* MSD for three different aerosol concentrations: clean (a), optimal (b), and polluted (c) for the deepest profile. The specific concentrations are noted on the upper left corner of each panel.

Text S4. The *Atlantic–1* MSD has no N_{op}. Additional sensitivity simulations were performed to examine the *Atlantic–1*'s MSD behavior under extremely polluted conditions. Figure S4 shows the same as Fig. 2a–b in the main text, but includes four additional simulations for the *Atlantic–1* MSD under N_{tot} of 10^4, 4×10^4, 10^5, and $10^6\,cm^{-3}$. From the Figure, it is clear that a N_{op} does not exist for the *Atlantic–1* MSD.

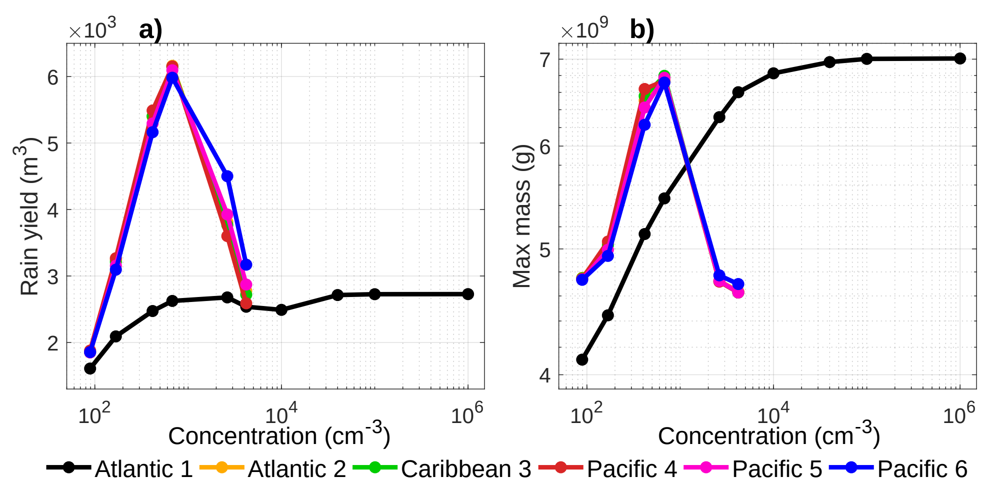

Figure S4. (a) Surface rain yield and (b) cloud's maximum mass as a function of N_{tot} used in the simulation. Each curve represents six simulations, performed with a specific shape of the MSD normalized to a different N_{tot}, except for the *Atlantic–1* MSD that is comprised of 10 simulations up to an aerosol concentration of $10^6\,cm^{-3}$.

Text S5. Total Droplet Surface Area Evolution. The temporal evolution of the total droplet surface area (summed over all cloudy pixels) was investigated for all MSDs, for four different N_{tot} (Fig. S5). The more polluted the clouds were (going from **a** to **d** in Fig. S5), the greater the difference in total droplet surface area between the *Atlantic–1* MSD and the rest of the MSDs. This is explained by the fact that the *Atlantic–1* MSD contained an UGCCN mode, and as N_{tot} increased, the amount of UGCCN also increased (see Fig. S1), reducing the total droplet surface area.

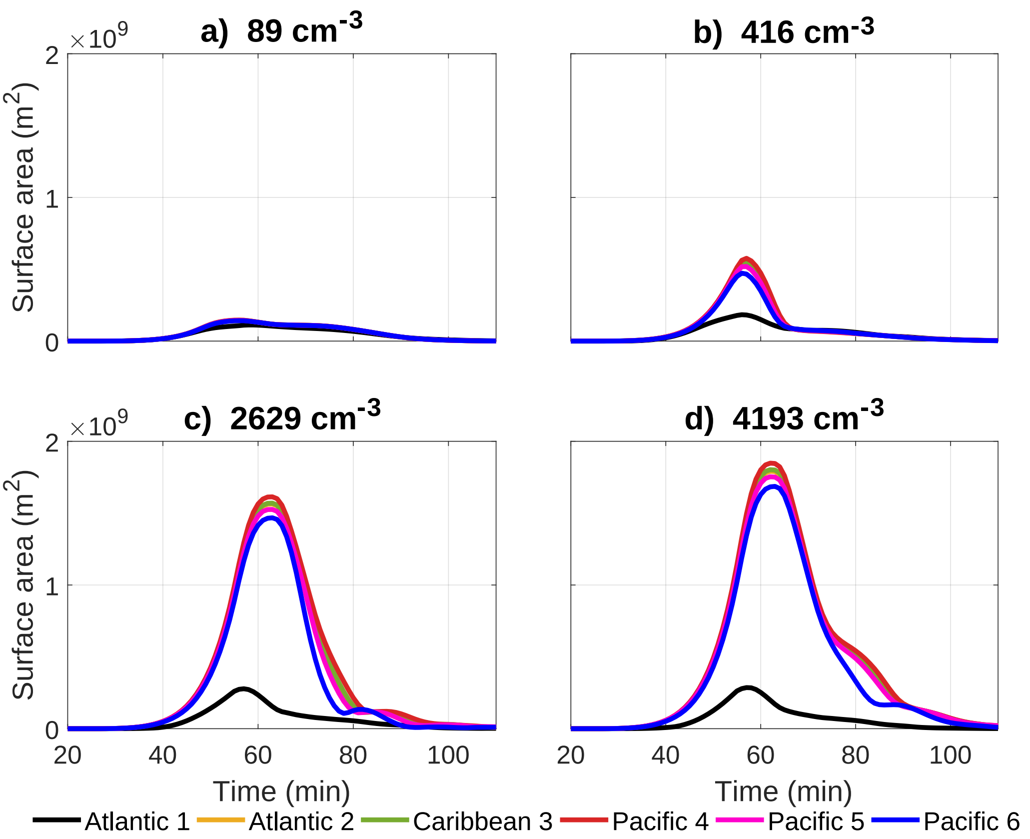

Figure S5. Total droplet surface area for N_{tot} of (a) $89\,cm^{-3}$, (b) $416\,cm^{-3}$, (c) $2629\,cm^{-3}$ and (d) $4193\,cm^{-3}$.

Text S6. Droplet Size Distribution Below the Cloud Base. To understand the reduced surface rain caused by the enhanced evaporation below the cloud base of the *Atlantic–1* MSD shown in Fig. 3 of the main text, we calculated the mean droplet size distribution for the time of maximum rain for an area just below cloud base. Figure S6 shows the droplet size distribution for all of the MSDs for $N_{tot} = 2629\,cm^{-3}$. The biggest droplets in the *Atlantic–1* MSD case are about six orders of magnitude less in concentration compared to the other five MSDs, explaining the more efficient evaporation below cloud base.

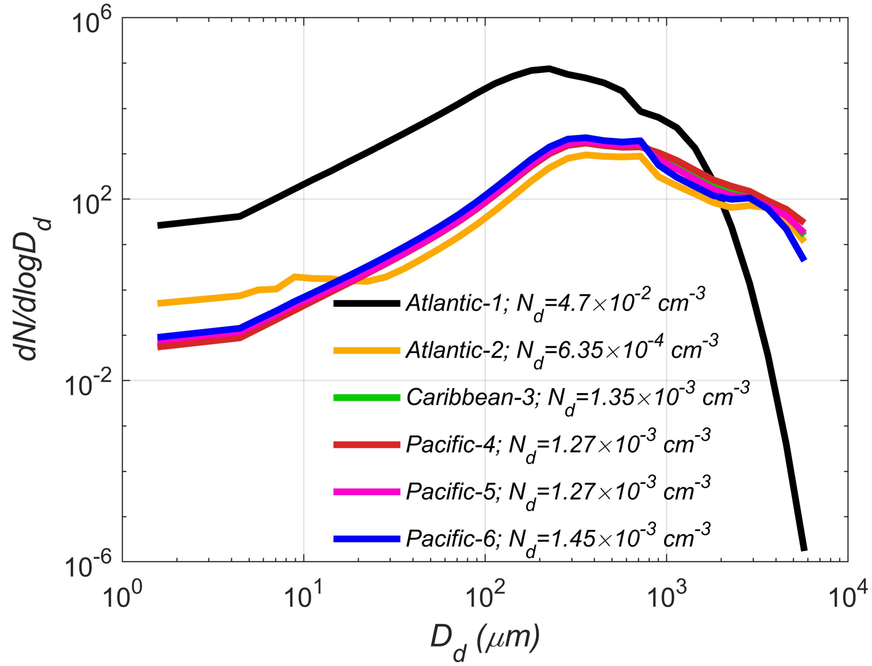

Figure S6. Droplet size distribution below the cloud base at the time of maximum surface rain rate for the six different MSDs normalized to $N_{tot} = 2629\,cm^{-3}$. The total droplet number concentration (N_d, cm^{-3}) is noted in the legend for each MSD.

Text S7. Time–height Diagrams of Cloud Mean properties. To understand the vertical distribution of some of the cloud's key properties, we show the time evolution of the cloud mass mixing ratio, droplet number concentration (N_d), vertical velocity (w), and relative humidity (RH) below the cloud mass of the *Atlantic–1* and the *Pacific–6* MSDs normalized to $N_{tot} = 2629\,cm^{-3}$. We show the *Pacific–6* MSD case as a representative example to the other four MSD cases, since their results are very similar. It is clear that while the *Atlantic—1*'s mass is the same order of magnitude as the one of the *Pacific–6*, the total N_d is considerably smaller for the *Atlantic–1* cloud, and that the droplets are confined to the lower part of the cloud. These are big droplets that nucleated on the GCCN and the UGCCN in the *Atlantic–1* MSD. These droplets sediment out almost immediately after their formation, thus are not carried to higher levels in the cloud. The *Atlantic–1* starts to precipitate earlier than the other clouds (as discussed in the main text), while the cloud is still in its developing stage, updrafts prevail and the sub—cloud layer features low RH values.

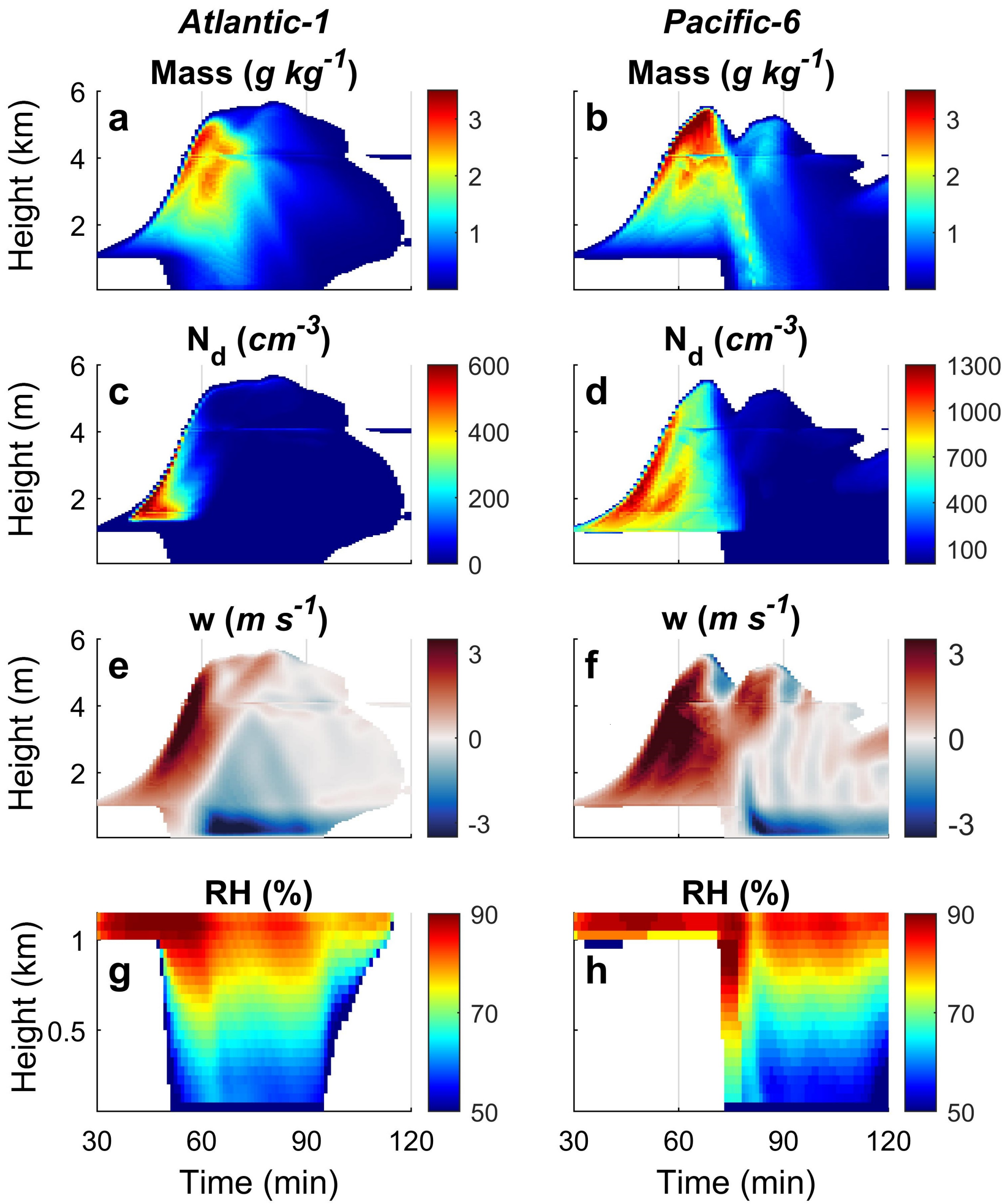

Figure S7. Time-height diagram of the horizontal mean of (a,b) cloud mass mixing ratio ($g\,kg^{-1}$), (c, d) droplet number concentration (N_d, cm^{-3}), (e, f) vertical velocity (w, $m\,s^{-1}$), and (g, h) relative humidity (RH, %) below the cloud base, for the *Atlantic–1* (left column) and *Pacific–6* (right column) MSDs normalized to $N_{tot} = 2629\,cm^{-3}$. Values are shown only for the cloudy (and rainy) pixels (mixing ratio $> 10^{-3} g\,kg^{-1}$). Note the different scales for the color bars in panels (c) and (d).

Text S8. Time–height Diagrams of Precipitating Particle's Growth. For clarifying the reasons behind the reduced surface rain amounts that are observed in the *Atlantic—1* MSD case, Fig. S8 shows the time-height evolution of the horizontal mean profiles of raindrops number concentration $N_r(D_p > 80\,\mu m)$, and mass mixing ratio $M_r(D_p > 80\,\mu m)$, for the *Atlantic–1* and the *Pacific–6* MSDs normalized to $N_{tot} = 2629\,cm^{-3}$. The formation of raindrops is observed at a very early stage of the *Atlantic–1* cloud lifetime, compared to the timing of the rain formation in the *Pacific–6* case. In addition, it is clear that the high N_r around the *Atlantic—1*'s cloud base contains very little mass, but the drops are big enough to fall out. However, since the drops are small, and the sub—cloud layer is still dominated by updrafts (Fig. S7e–f) the majority of them evaporate before reaching the surface (efficient evaporation and longer fall time).

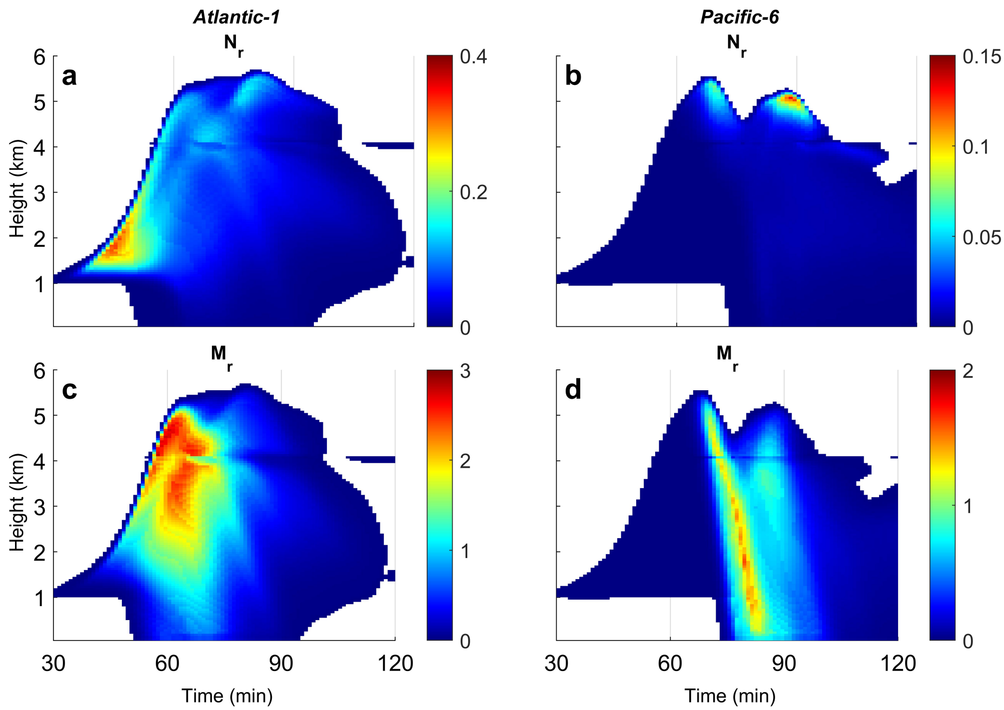

Figure S8. Time–height diagram of the horizontal mean of raindrops ($D_p > 80\,\mu m$) (a, b) number concentration (N_r, cm^{-3}) and (c, d) mass mixing ratio (M_r, $g\,kg^{-1}$), for the *Atlantic–1* (left column) and *Pacific–6* (right column) MSDs normalized to $N_{tot} = 2629\,cm^{-3}$. Values are shown only for the cloudy (and rainy) pixels (mixing ratio $> 10^{-3} g\,kg^{-1}$). Note that the color bars have different limits for the *Atlantic–1* and *Pacific–6* clouds.

References

Dagan, G., Koren, I., and Altaratz, O.: Competition between core and periphery-based processes in warm convective clouds–from invigoration to suppression, Atmospheric Chemistry and Physics, 15, 2749–2760, 2015.

Garstang, M. and Betts, A. K.: A review of the tropical boundary layer and cumulus convection: Structure, parameterization, and modeling, Bulletin of the American Meteorological Society, 55, 1195–1205, 1974.

Pinsky, M., Mazin, I., Korolev, A., and Khain, A.: Supersaturation and diffusional droplet growth in liquid clouds, Journal of the Atmospheric Sciences, 70, 2778–2793, 2013.

Seiki, T. and Nakajima, T.: Aerosol effects of the condensation process on a convective cloud simulation, Journal of the Atmospheric Sciences, 71, 833–853, 2014.